Femtosecond dynamics of solvated oxygen anions. II. Nature of dissociation and caging in finite-sized clusters

Nam Joon Kim, D. Hern Paik, and Ahmed H. Zewail

Citation: The Journal of Chemical Physics **118**, 6930 (2003); doi: 10.1063/1.1561434
View online: http://dx.doi.org/10.1063/1.1561434
View Table of Contents: http://scitation.aip.org/content/aip/journal/jcp/118/15?ver=pdfcov
Published by the AIP Publishing

Femtosecond dynamics of solvated oxygen anions. II. Nature of dissociation and caging in finite-sized clusters

Nam Joon Kim, D. Hern Paik, and Ahmed H. Zewail[a)]
Arthur Amos Noyes Laboratory of Chemical Physics, Laboratory for Molecular Sciences, California Institute of Technology, Pasadena, California 91125

(Received 10 October 2002; accepted 23 January 2003)

Ultrafast dissociation and recombination dynamics of $(O_2)_n^-$, $n=3-10$ was studied using femtosecond, time-resolved photoelectron spectroscopy. The observed transients of nascent fragment anions, following 800 nm fs pulse excitation, exhibit a biexponential rise with two distinct time constants. The time constants, which vary with the number of solvent O_2 molecules, clearly show the solvation effect in two different dissociation pathways. Consistent with the bifurcation picture in the preceding paper, the direct subpicosecond dissociation ($\tau_1=110-620$ fs, depending on n) is governed by electron recombination and kinematics of the half-collision. The second pathway is indirect ($\tau_2=0.7-8.0$ ps, for O_6^- to O_{20}^-) and controlled by intramolecular vibrational-energy redistribution. In the solvent cage, only O_{16}^-, O_{18}^-, and O_{20}^- show the reformation of the bond, with the caging time constant decreasing from 4 ps for the first two to 2 ps for the latter. This caging through ion-induced dipole interaction is then followed by vibrational relaxation on the time scale of 12 to 3 ps, for O_{16}^- to O_{20}^-. The time scale for the initial direct caging is two to five times slower than that previously observed for diatoms, neutral, or ionic, in van der Waals clusters. We suggest that this initial slower caging is due to the reorientation of O_2^- and O_2 to acquire a proper geometry for O_4^- bond reformation. In these finite-sized homogeneous clusters, we compare theory with experiment. We also found a correlation between the vertical detachment energy and $n^{-1/3}$, for n in the range of 2–10, which allow for a connection between the mesoscopic structures and a bulk-type dielectric continuum, with an effective dielectric constant. © *2003 American Institute of Physics.* [DOI: 10.1063/1.1561434]

I. INTRODUCTION

At the molecular level, van der Waals (vdW) clusters have been considered as an ideal system to understand the solvation effect on dissociation and recombination dynamics. Since the proposal for caging by Franck and Rabinowitsch in 1930,[1] intensive efforts have been made to understand the recombination in solution, in vdW clusters and in dense fluids (see Refs. 2–4 and references therein). Photoelectron (PE) spectroscopy of mass-selected anionic clusters makes possible the study of solvation systematically by increasing the number of solvent atoms or molecules. Prototypical examples include the $Br_2^-(CO_2)_n$ and $I_2^-(CO_2)_n$ clusters, which were investigated both experimentally[5–10] and theoretically.[11–14] Neutral clusters were studied in this laboratory with focus on the time scale for the initial coherent caging and subsequent vibrational relaxation in solvent cages.[15–17] However, studies of recombination have been mostly devoted to diatomic solute molecules in solvent clusters.

In this work, we investigate solvation effect on the dissociation and recombination dynamics by varying the number of solvent molecules in a homogeneous series of O_2^- clusters. The femtosecond (fs), time-resolved PE spectroscopy was used to follow the reaction dynamics of $(O_2)_n^-$, $n=3-10$ in real time, following excitation with 800 nm fs pulse. Two distinct time constants were obtained in the transient monitoring nascent fragment anions. The change of both time constants with the cluster size shows the different role of solvation in the two dissociation pathways, direct and indirect, discussed in the preceding paper.[18] The caging effect by the solvent is evident on the time scale of the direct dissociation, when the cluster size exceeds the threshold of O_{16}^-. For the indirect process, which occurs on a longer time scale than that of caging, the total rate is controlled by the redistribution of energy and vibrational predissociation. We compare theory with experiments, deducing correlations that provide a connection to bulk-type behavior and to the electron transfer mechanism.

II. EXPERIMENTAL

The experimental apparatus was discussed previously,[18,19] and only a brief description is given here. The O_2^- clusters were produced by secondary electron attachment during the supersonic expansion of a gas mixture (approximately 90% oxygen and 10% Ar) at total backing pressure of 95 psig. The anionic clusters were collimated by the skimmer and then entered a two-stage accelerator. The ion bunches were accelerated by a pulsed high electric field (-2.0 kV) into a field-free region, where the different masses of clusters were separated by their flight time.

The cluster of interest was irradiated by fs laser pulses, which produced photofragments and photoelectrons. The fragment ions were analyzed by a linear reflectron time-of-

a)Electronic mail: zewail@caltech.edu

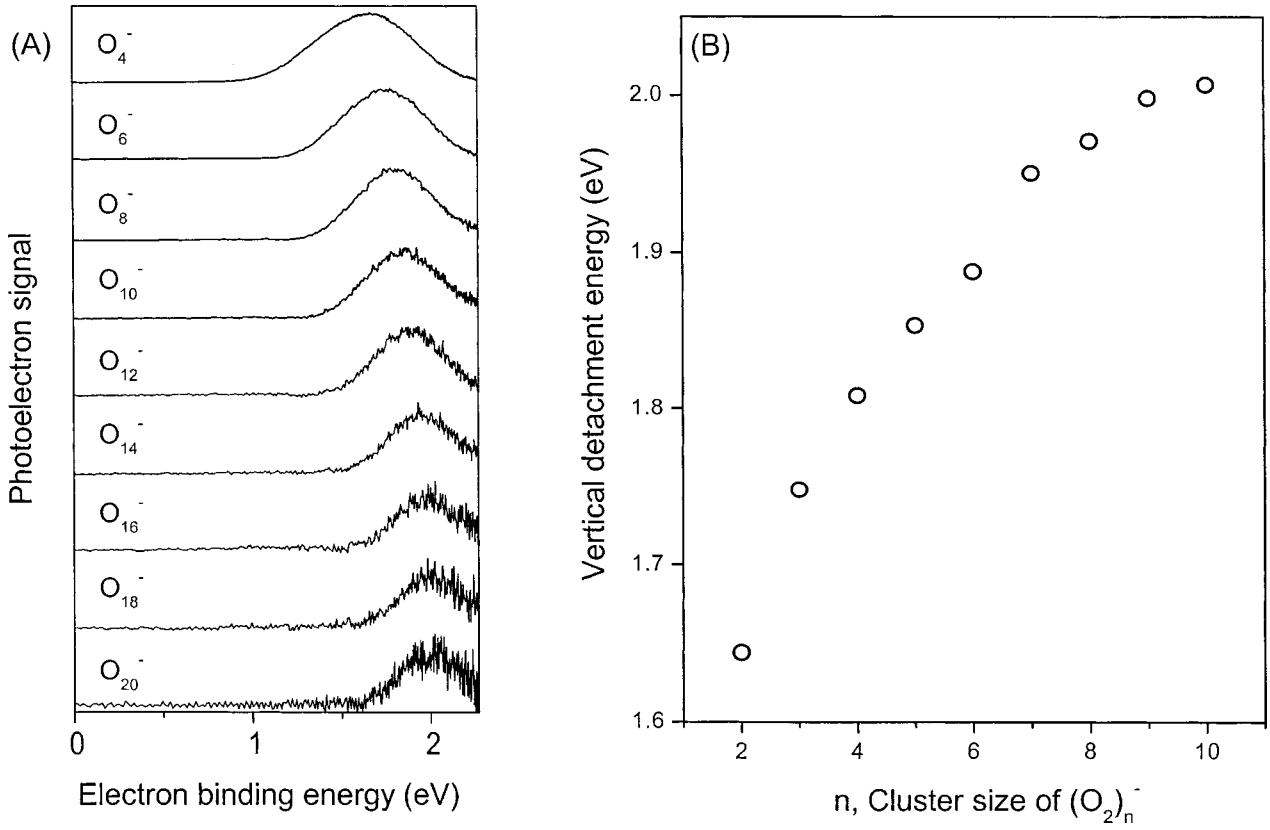

FIG. 1. (a) PE spectra of $(O_2)_n^-$, $n=2-10$ obtained by excitation at 400 nm with a fs pulse. (b) A plot of VDE vs cluster size n.

flight mass spectrometer, and the photoelectrons were collected by a magnetic-bottle PE spectrometer. To prevent multiphoton processes while maximizing the overlap between the laser pulses and the ion beam, the laser beam was collimated only to a 5 mm diameter in the laser interaction region.

The fs laser pulse at 800 nm (1.55 eV) was generated from a Ti:sapphire oscillator. This output was amplified up to 6 mJ/pulse by a regenerative and a multipass amplifier. The amplified output was frequency doubled by a BBO crystal, generating 800 μJ/pulse at 400 nm (3.1 eV). The remaining 800 nm output of 1.5 mJ/pulse was used as a pump pulse to dissociate O_2^- clusters, while an optically delayed 400 nm laser pulse was used as a probe to detach the electron from the nascent fragment anion.

Based on studies of the power dependence of the pump pulse, the possibility of multiphoton processes was excluded because of the following: First, we observed a slope of ~ 0.5 in the plot of log(signal) versus log(I_{pump}), consistent with previous nanosecond work,[20] indicating a one-photon absorption (linear) and one-photon absorption/one-photon depletion by the same 800 nm wavelength; if two 800 nm pump photons are involved in the dissociation of the cluster (followed by 400 nm probe photodetachment of O_2^-), then the slope will be $\geqslant 1$, with a maximum n value of 2. Second, we also recorded the transient behavior at half the pump power and observed the same transients. Third, if the fast component is due to two pump photons to the higher-energy repulsive potential, we do not expect the dramatic change observed for the rates of $(O_2)_n^-$. Accordingly, the transient signal reported here is for a one-photon excitation at 800 nm, followed by a one-photon detachment at 400 nm (generated by SHG).

III. RESULTS

Figure 1(a) shows the PE spectra of O_2^- clusters using a 400 nm fs laser pulse. The vertical detachment energy (VDE) of each cluster is determined by fitting the observed peak to a single Gaussian function. The values obtained are plotted as a function of cluster size [Fig. 1(b)]. The increase of VDE with n indicates that the anionic clusters become more stable, compared to the corresponding neutral ones, as the number of O_2 molecules increases. As shown below, the plot of the VDE against $n^{-1/3}$, where n is the number of O_2 molecules of the negative ion cluster, follows the linear equation of $\mathrm{VDE}=2.53-1.13\times n^{-1/3}$. The correlation gives a bulk value of the VDE (2.53 eV), when an electron is solvated by ''infinite number'' of O_2 molecules.[21]

The overall shape of the PE spectra [Fig. 1(a)] resembles that of O_4^-, suggesting that additional O_2 molecules bind to O_4^- by weak interactions. The gradual increase of VDE without any abrupt shift [Fig. 1(b)] implies no structural change in these clusters.[22] In addition, the fact that all of the PE spectra are well fitted to a single Gaussian profile indicates that no other structural isomers with a different core ion coexist, at least within our resolution. From these results, we conclude that the O_2^- clusters have a unique structure where O_4^- is a dimeric core, and the rest of the O_2 molecules form a solvent shell, which is consistent with previous observations.[19,20,23]

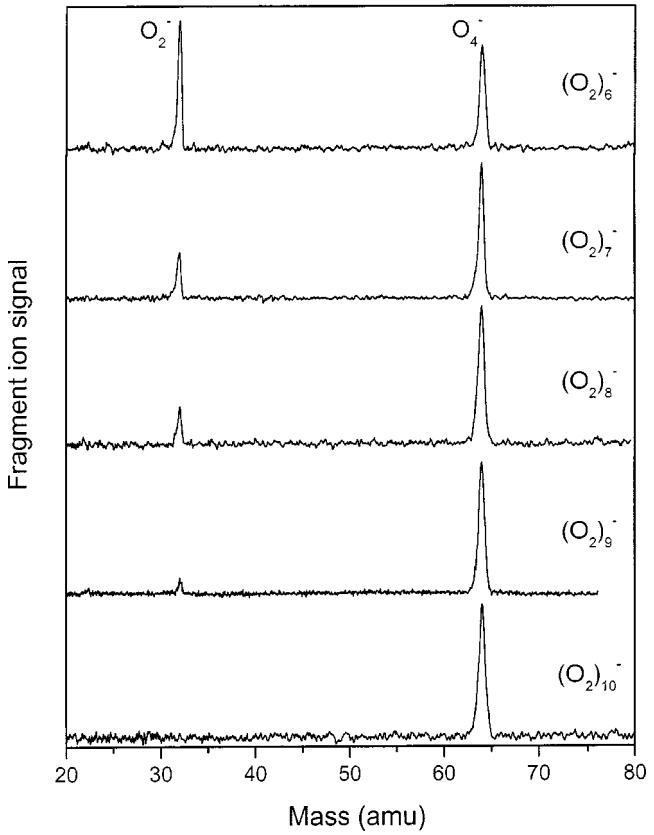

FIG. 2. Fragment mass spectra observed from the dissociation of $(O_2)_n^-$, $n=6-10$ using a 800 nm fs pulse. These mass spectra were obtained using the linear reflectron time-of-flight mass spectrometer. The parent cluster corresponding to each fragment spectrum is indicated on the right-hand side.

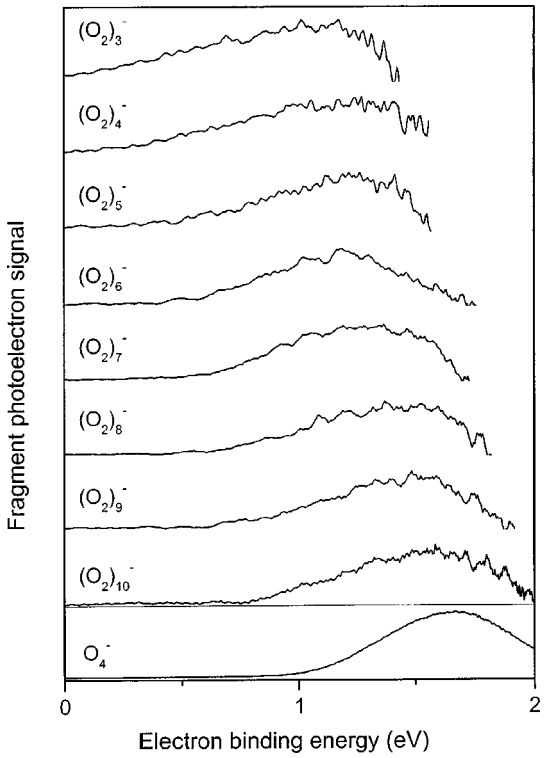

FIG. 3. Fragment PE spectra obtained from the differential fs pump/probe signal at 400 ps time delay and at time zero. The PE spectrum of O_4^- (400 nm probe pulse only) is shown at the bottom for comparison. The parent anion corresponding to each fragment PE spectrum is indicated on the left-hand side.

Figure 2 shows fragment mass spectra of parent $(O_2)_n^-$, $n=6-10$, obtained upon irradiation with a 800 nm fs pulse. In our earlier communication, we reported that the major anionic fragment in $(O_2)_n^-$, $n=3-5$ was found to be O_2^-, and the intensity of O_4^- was found to increase as the cluster size was increased.[19] This trend continues here for larger clusters. The intensity ratio of O_4^- to O_2^- becomes larger, reaching the 100% level for $(O_2)_{10}^-$, as shown in the figure. No anionic fragments other than O_2^- and O_4^- were detected.[24]

Figure 3 shows the *fragment* PE spectra obtained from the pump/probe PE spectrum at a 400 ps time delay between the pump (800 nm) and probe (400 nm) pulses minus the pump/probe PE spectrum at time zero. The PE spectrum of O_4^- with a 400 nm probe pulse only is also shown for comparison. The envelope of the PE signal, as well as its onset, shifts toward higher electron binding energy (EBE) as the parent cluster size increases.

The transients obtained by detecting fragment anions are shown in Fig. 4. The transients were recorded by integrating the entire PE signal of nascent fragment anions (shown in Fig. 3). We fitted the data to a biexponential rise, varying the amplitude (A_1 and A_2) and time constants (τ_1 and τ_2). The response function was included using the autocorrelation function of the pulse width (110 fs) at 800 nm. We also checked for the values of the fit without convolution and obtained similar values for τ_1, τ_2, and γ. Figure 5 depicts the behavior of the values of k_1 $(1/\tau_1)$ and k_2 $(1/\tau_2)$ as a function of n.

We note that the nascent fragment anions generated in the dissociation of large O_2^- clusters at 800 nm are not only O_2^- but also solvated O_2^-, i.e., $O_2^-(O_2)_m$ $(m<n-1)$. The $O_2^-(O_2)_m$ subsequently transforms to O_2^- or O_4^- by evaporative dissociation, which are the only fragments observed in our reflectron time-of-flight ($\sim 20\ \mu$s) mass spectrometer. The existence of the fragment $O_2^-(O_2)_m$ is evidenced by the onset of the PE envelope in Fig. 3, which was obtained at a 400 ps time delay. The onset is shifted toward higher EBE by 0.1–0.3 eV with respect to that of cold O_2^-, which was attributed to the stabilization of O_2^- by the solvation with O_2 molecules.

Unlike O_4^-, where an excess electron is delocalized between two O_2 species, the electron in $O_2^-(O_2)_m$ is localized at one O_2. The onset of O_4^- is 0.5 eV, shifted to the higher EBE with respect to that of O_2^-, while the shift of $O_2^- \cdot O_2$ is not known experimentally. However, from the onset shift of $O_2^- \cdot N_2$ (0.26 eV),[25] we can roughly estimate the shift to be about 0.24 eV. With this estimated value, our probe window covered the region where the PE signal from $O_2^-(O_2)_m$, $m \leqslant 5$ could be detected. In order to separate different contributions from $O_2^-(O_2)_m$ to the transients, we positioned a narrow gate at several different regions of the fragment PE envelope; the time constants were about the same. This is consistent with a significant overlap in the broad PE spectra of $O_2^-(O_2)_m$.

Figure 6 shows a series of time-dependent PE spectra at

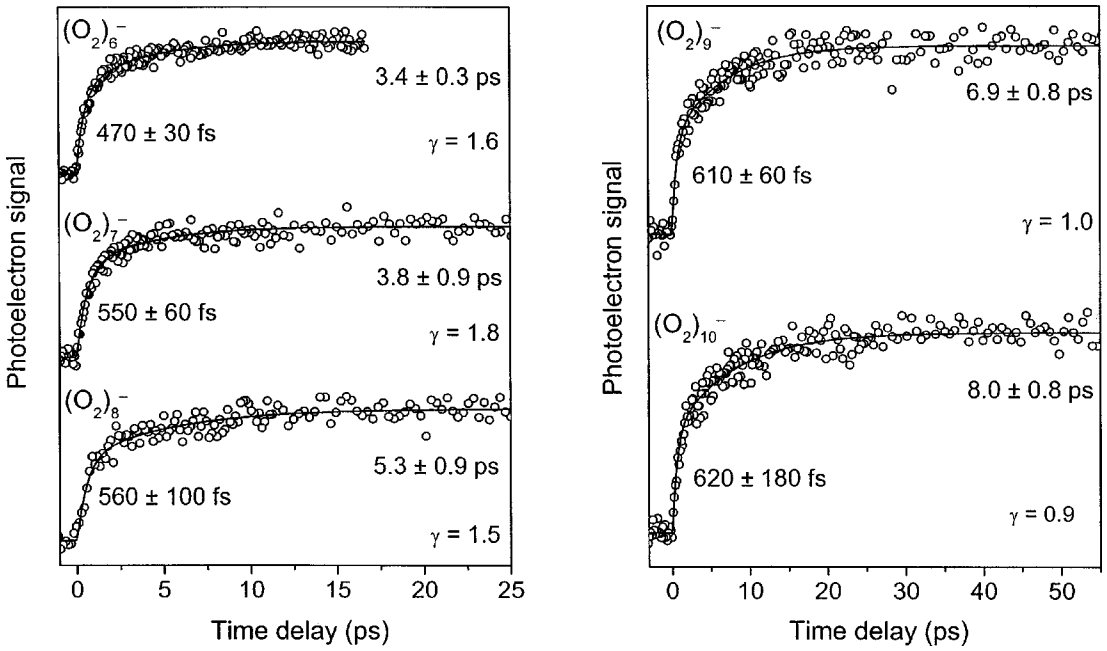

FIG. 4. Femtosecond transients obtained by monitoring the fragment anions in the dissociation of $(O_2)_n^-$, $n=6-10$ at 800 nm. All transients were fitted to a biexponential function. The τ_1 and τ_2, and the ratio of amplitudes, $\gamma\,(\equiv A_1/A_2)$, are indicated for each of the parent anions shown.

different time delays. Each PE spectrum is constructed by subtracting the pump/probe PE spectrum at time zero from the pump/probe PE spectrum at a certain time delay. In Fig. 6, several representative spectra are presented from a dataset, consisting of 20 measurements in order to clearly show the time-dependent behavior. For $(O_2)_6^-$ and $(O_2)_7^-$, the peak of fragment PE spectra shifts toward lower EBE with time. However, for $(O_2)_8^-$, $(O_2)_9^-$, and $(O_2)_{10}^-$ the peak moves at first toward lower EBE and then at 2–4 ps time delay the shift turns its direction toward higher EBE.

The peak positions were determined either from the pump/probe PE spectrum, which have the PE signals from both fragment and parent anions (each as a Gaussian), or from the fragment change represented by the rise of the fragment and depletion of the parent (each as a Gaussian). The behavior is shown in Fig. 7. We then obtained the rate at which the EBE is decreasing or increasing by fitting the change in the fragment peak position as a function of time to an exponential decay or rise, respectively. The time-dependent variation of the peak position is plotted in Fig. 8.

IV. DISCUSSION

Two different pathways following the bifurcation of the initial wave packet were shown in the early communication

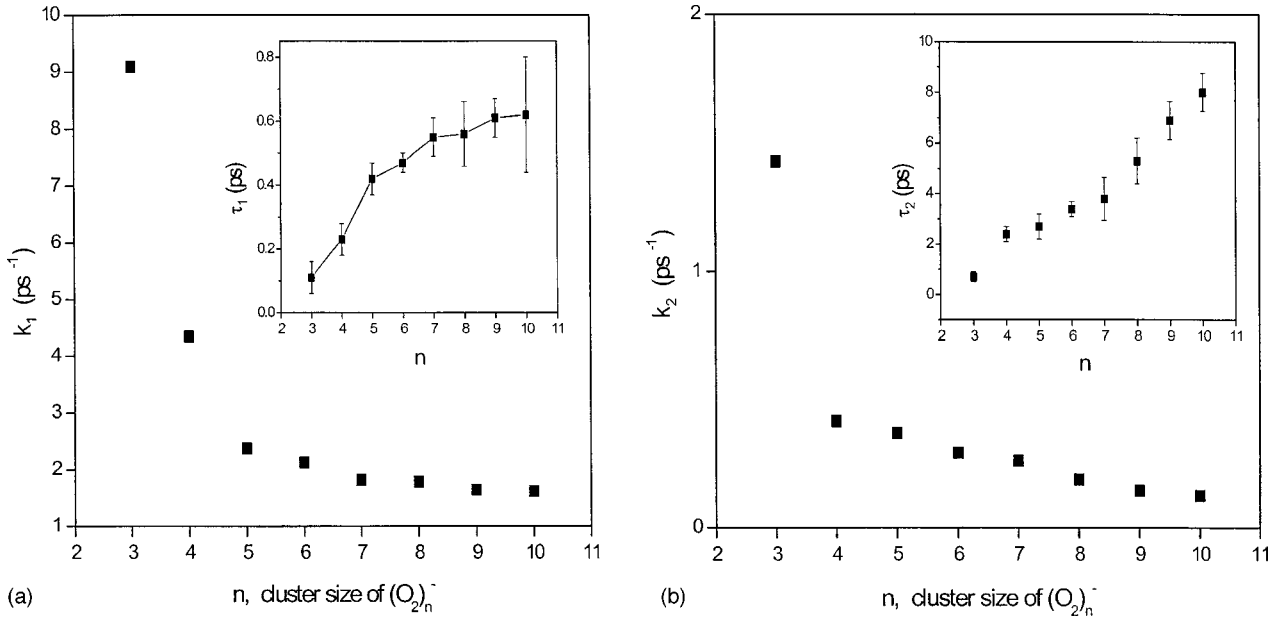

FIG. 5. (a) A plot of k_1 vs cluster size n. (b) A plot of k_2 vs n. The inset in each panel gives the corresponding dependence for τ_1 and τ_2.

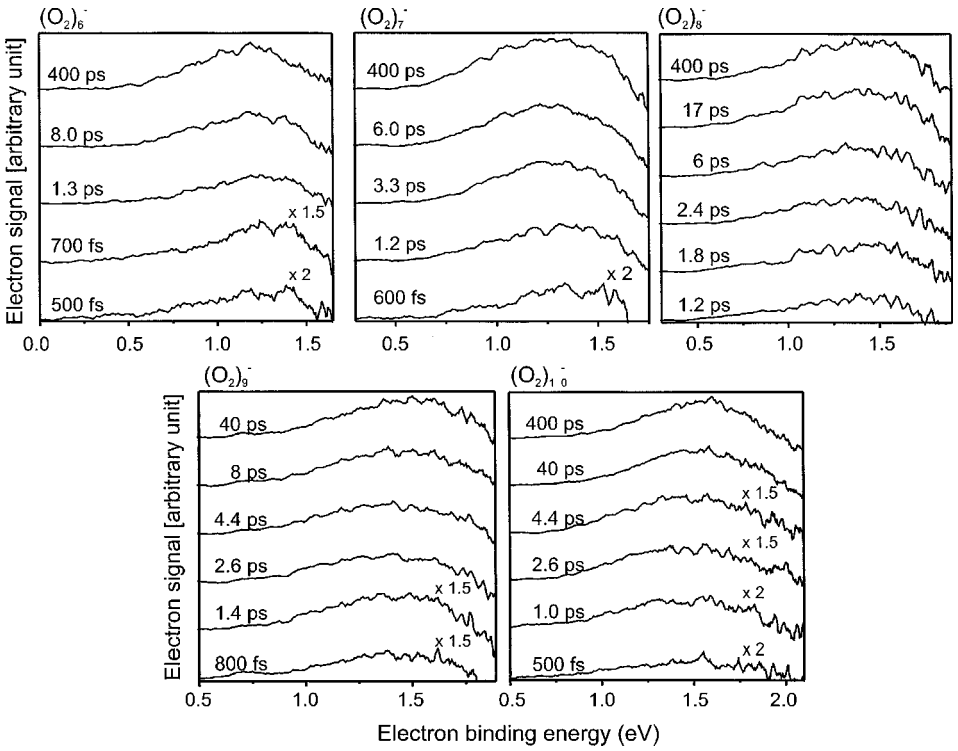

FIG. 6. Time-dependent fragment PE spectra with the time delays indicated. The spectra were obtained as a differential pump/probe PE at the time delay given and that of time zero.

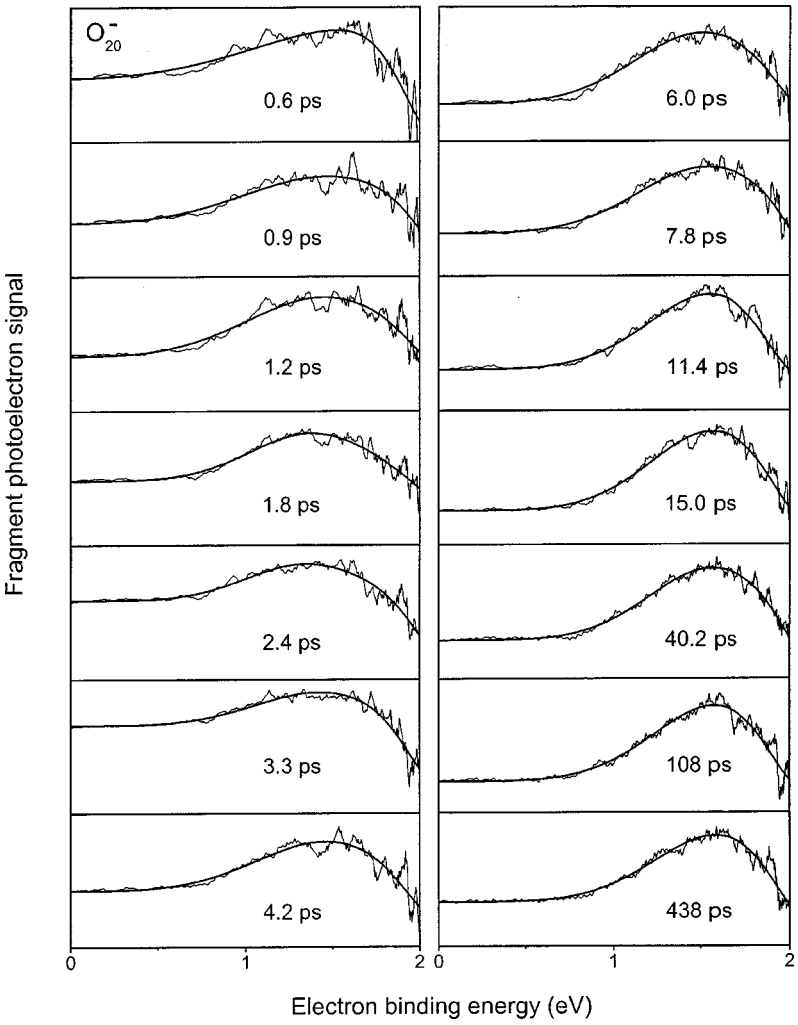

FIG. 7. Time-dependent fragment PE spectra of parent O_{20}^-. The solid line is a Gaussian profile (see the text for details).

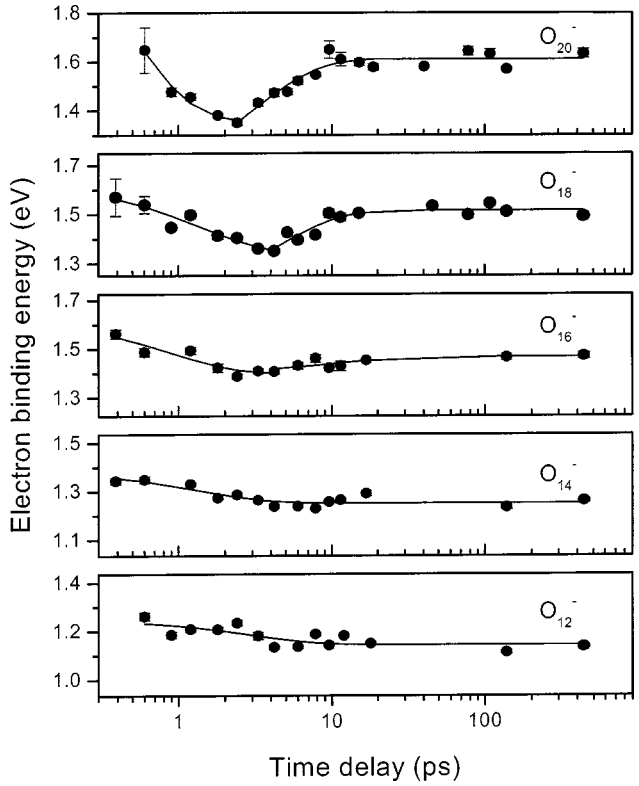

FIG. 8. A plot of the peak position in the fragment PE spectrum as a function of the time delay. The error bars are indicated for the peak position (see the text). The solid line is a fit to indicate the rate at which energy changes with time (see the text).

and in the preceding paper to account for the observations made in all systems studied. For the larger clusters, the same picture holds because of the following findings: First, as discussed above, O_4^- remains a dimeric core. Second, the pump pulse energy (1.55 eV) is sufficiently high to compensate for any stabilization by additional solvent molecules. Third, the transient exhibits two distinct rises with time constants vastly different and depend on the cluster size. In what follows we consider the dynamics in these two channels and the effect of microscopic solvation.

A. Electron transfer and solvation

As discussed in Paper I, the initial process can be written as

$$O_4^- \cdot O_2 + h\nu \rightarrow O_4 \cdot O_2^{-*\ddagger} \xrightarrow{\text{direct (ER)}} O_2^- + 2O_2. \tag{1}$$

Thus, τ_1 is the joint time constant for electron recombination and the nuclear motion that follows in dissociation. The electron recombination is on the fs time scale and occurs without involving major reorganization of molecules in the cluster. However, the addition of solvent molecules slows down the process by breaking the resonance between the reactant $O_2^- \cdot O_4$ and the product $O_2 \cdot O_4^-$. Moreover, solvation will result in some charge delocalization and the weaker coupling is expected to increase the separation between O_2^- and O_4. Both the asymmetry and separation changes will affect the energetics of the HOMO (O_2^-) and the LUMO (O_4).[26] The deceleration in the electron recombination is a significant factor in the increase of τ_1, from O_6^- to $O_6^- \cdot X$.[18,19] As the cluster size increases, we also expect the nuclear motion to be affected by the solvent confinement, as discussed elsewhere.[27] Below we shall discuss the change in τ_1, with cluster size.

B. From clusters to bulk

In this section we consider the change in rates and vertical detachment energy as the cluster size increases. Bowen and his co-workers[28] obtained VDE of solvated anion clusters $O^-(Ar)_{n=1-26,34}$ and estimated bulk parameters, such as the photoemission threshold, the photoconductivity threshold, and the bulk solvation energy. The theory by Jortner[29] makes the connection between cluster and bulk energetics. The expressions for VDE and the adiabatic electron affinity (AEA) have the $n^{-1/3}$ dependence that relates to the inverse of the radius of cluster for different n:

$$\text{VDE}(n) = \text{VDE}(\infty) - An^{-1/3}, \tag{2a}$$

$$\text{AEA}(n) = \text{AEA}(\infty) - Bn^{-1/3}, \tag{2b}$$

where the values at infinity are those of the bulk. The slope is given by

$$A = \frac{e^2}{2R_0}\left(1 - \frac{2}{\epsilon_0} + \frac{1}{\epsilon_\infty}\right), \tag{3a}$$

$$B = \frac{e^2}{2R_0}\left(1 - \frac{1}{\epsilon_0}\right), \tag{3b}$$

where e is the charge, R_0 is the effective radius of the solvent, ϵ_0 is the static dielectric constant, and ϵ_∞ is the corresponding high-frequency dielectric constant.

In Fig. 9 we present our data as plots of VDE and AEA of $(O_2)_n^-$, $n=2-10$ against $n^{-1/3}$. A linear relationship was obtained giving the following intercepts and slopes:

$$\text{VDE}(n) = 2.53 - 1.13n^{-1/3}, \tag{4a}$$

$$\text{AEA}(n) = 2.33 - 1.79n^{-1/3}. \tag{4b}$$

For the AEA of $(O_2)_n^-$, we used the values in Refs. 20 and 23, for $n=2-6$; for the larger clusters, we obtained them from the PE spectra given in Fig. 1(a). For our system, with $R_0 = 2.13$ Å, which is deduced from the bulk density of liquid O_2,[30] we obtained $\epsilon_0 = 2.13$ and $\epsilon_\infty = 3.65$. From the intercepts, we obtained the "bulk values" of VDE (2.53 eV) and AEA (2.33 eV). These values represent effective bulk parameters extrapolated to from the mesoscopic properties of clusters. It is interesting that our ϵ_0 of 2.13 is larger than the bulk value of 1.568.[30]

For the rates the behavior as a function of n is not linear, as shown in Fig. 5(a). We replotted the data in Fig. 10 to show the experimental behavior obtained for k_1 versus $n^{1/3}$, which is related to the radius of the cluster by $R = R_0 n^{1/3}$. The agreement is surprisingly good and gives the following relationship:

$$k_1 = 1.57 + 7.6\exp(-7.3(n^{1/3} - 3^{1/3})) \tag{5}$$

where k_1 is in units of ps^{-1} and $3^{1/3}$ is related to the cluster radius of O_6^-, which is the smallest cluster that undergoes

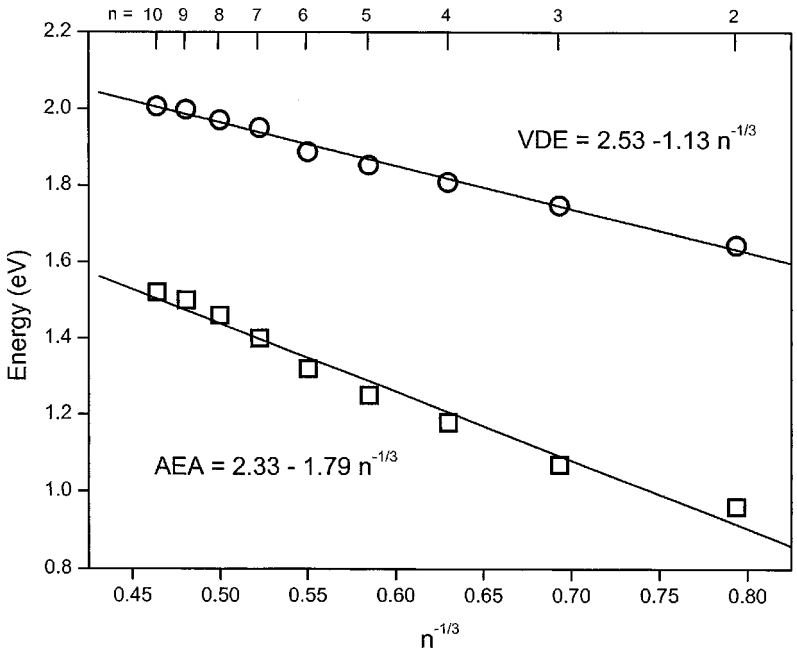

FIG. 9. The experimental and theoretical fits for the change of vertical detachment energy (VDE) and adiabatic electron affinity (AEA) against $n^{-1/3}$. The best values are shown.

recombination. The distance dependence is governed by the exponential form, and the value for ''infinite'' separation is the residual $1.57\,\mathrm{ps}^{-1}$ (0.64 ps); the maximum value is $9.17\,\mathrm{ps}^{-1}$ (0.11 ps). Considering the R_0 value of O_2, we obtained the form $7.6\exp(-\beta(r-r_m))$, with $\beta\sim 3\,\text{Å}^{-1}$, and a pre-exponential of $7.6\times 10^{12}\ \mathrm{s}^{-1}$ ($250\ \mathrm{cm}^{-1}$). It is interesting to note the analogy with electron transfer in solution, where β is typically $1.5\,\text{Å}^{-1}$, in DNA that is less than $1\,\text{Å}^{-1}$, and in a vacuum that reaches $3-5\,\text{Å}^{-1}$ (see Refs. 31–33).

C. Evaporation and solvation

As discussed in Paper I, the second dynamical process involves energy redistribution and predissociation:

$$O_4^-\cdot O_2 + h\nu \rightarrow O_4\cdot O_2^{-*\ddagger} \xrightarrow{\text{indirect (IVR/VP)}} O_2^- + 2O_2. \qquad (6)$$

For this process, τ_2 is governed by the rate of intramolecular vibrational-energy redistribution among the vibrational modes of the cluster. Consequently, the plot of τ_2 as a function of cluster size is expected to exhibit quite a different behavior from that of τ_1. As shown in Fig. 5, except for an abrupt increase of τ_2 from $(O_2)_3^-$ to $(O_2)_4^-$, τ_2 gradually increases with the cluster size, without showing saturation behavior up to $n=10$.

The dynamics of vibrational predissociation has been extensively studied in size-selected dihalogen-rare gas clusters.[34–36] It is suggested that two pathways for vibrational-energy transfer determines the rates: One that in-

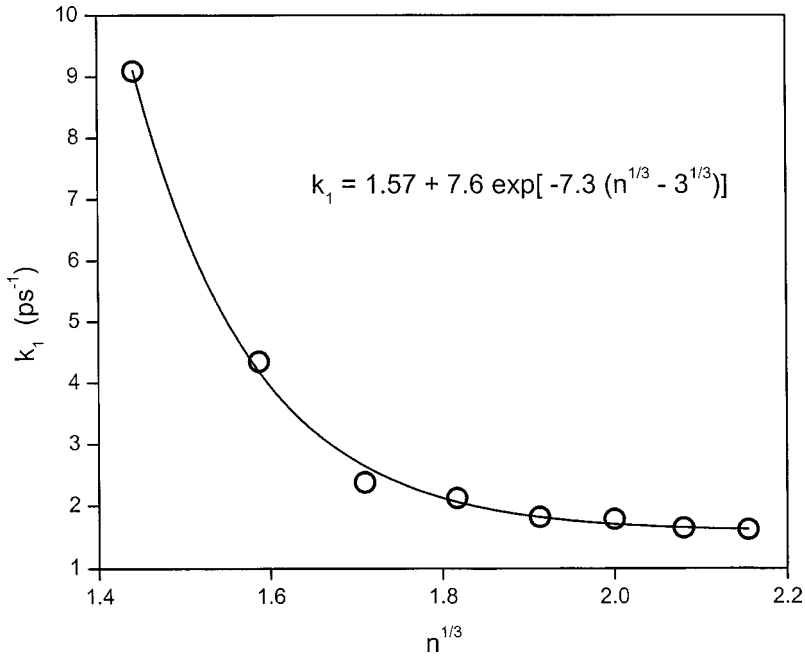

FIG. 10. The plot of k_1 vs $n^{1/3}$. The data are fitted to an exponential function with the best values given in the figure.

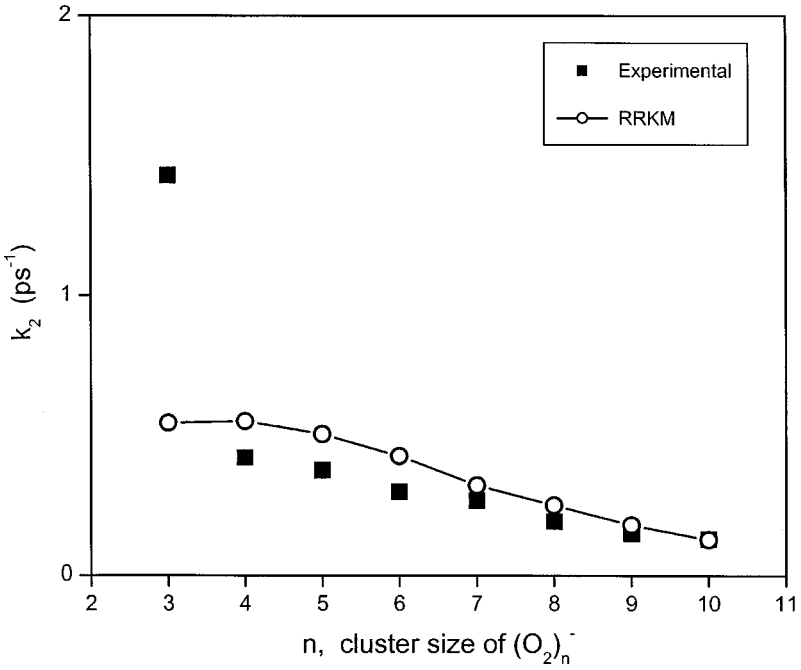

FIG. 11. The plot of k_2 vs n. The open circles are the calculated rates using RRKM theory and the solid squares are the experimental results.

volves direct energy transfer to the dissociative mode(s), i.e., direct vibrational predissociation (VP), while the other involves transfer of vibrational energy to nonreactive modes (IVR). Following this IVR, the energy in nonreactive modes is then channeled into the reaction coordinate.[36] In small clusters, VP is expected to be predominant, and the rate is governed by the coupling between the initially prepared bound state and the final dissociation continuum.[37] For larger clusters, with the increase of the density of states, IVR plays a more important role.[38] It was shown that more quanta were needed to eject the first rare gas atom as the size of cluster increases.[36] Since IVR increases with cluster size, large clusters may reach a statistical limit, and the rate of vibrational predissociation can be successfully described by a statistical theory.

To test this hypothesis, we used the RRKM (Rice–Ramsperger–Kassel–Marcus) theory[39] to calculate the rate constant:

$$\frac{1}{\tau_2} \equiv k_2 = \sigma \frac{N^{\sharp}(E-D)}{h\rho(E)}, \tag{7}$$

where σ is the degeneracy, h is Planck's constant, $N^{\sharp}(E-D)$ is the number of states at the transition state, and $\rho(E)$ is the density of states of the reactant. The reaction coordinate involves $O_2^-(O_2)_{n-1}$, which is a charge transferred partner of the parent $O_4^-(O_2)_{n-2}$. We obtained the optimized structure and the vibrational frequencies of $O_2^- \cdot O_2$ using the unrestricted Hartree–Fock level of theory with 6-311+G* as a basis set.[40] The calculated intermolecular frequencies of $O_2^- \cdot O_2$ were employed to obtain $N^{\sharp}(E-D)$ and $\rho(E)$.

In calculating the effective rate constant, k_2, we considered the following six dissociation channels:

$$(O_2)_n^- \rightarrow O_2^-(O_2)_{m-1} + (n-m)O_2, \quad m=1-6. \tag{8}$$

Following the initial evaporative dissociation, further dissociation may occur. However, subsequent dissociations will not appear in our transient because the photodetachment cross-section of the fragments is about the same. The PE signal of the fragments is integrated in our boxcar gate, which makes the probe insensitive to subsequent dissociations yielding smaller fragments.

In the above expression of k_2, E is the energy of the excitation pulse minus the difference in energy (at the minimum of the potential) between $O_2^-(O_2)_{n-1}$ and $O_4^-(O_2)_{n-2}$. We took E to be the same for all clusters since the stabilization energy by O_2 molecules is about the same for $O_2^- \cdot O_2$ and O_4^-. The transition state for the reaction generating O_2^- and $O_2^- \cdot O_2$ was considered to be a product type and the dissociation energy D was deduced using the value of AEA of O_2^- and the estimated stabilization energy by O_2. However, for the other channels yielding larger fragments, we assumed the same activation barrier height for the dissociation coordinate of $O_2^- \cdot O_2$. The σ value was 1 for the channel producing O_2^-, $(n-1)$ for channel producing $O_2^- \cdot O_2$, $(n-1)(n-2)/2!$ for channel producing $O_2^- \cdot 2O_2$, and so on.

The calculated rates are given in Fig. 11. The agreement between the theoretical and experimental trend is reasonably good, except for the smallest cluster $(O_2)_3^-$. This indicates that significant degree of IVR precedes VP for $(O_2)_n^-$ ($n \geqslant 4$), and that ''thermal'' evaporation is dominant. The overestimation of the degeneracy factor σ, because of the lack of direct information on the anionic structure of the clusters, may account for the somewhat larger rate constants obtained theoretically for $n \geqslant 4$.

D. Recombination and caging

The temporal behavior observed in the fragment PE spectra (Fig. 8) is consistent with previous observations in $I_2^-(Ar)_n$ and $I_2^-(CO_2)_n$ made by Neumark and his co-workers.[8,9] The shift toward lower EBE with time is at-

tributed to the evaporation of solvent O_2 molecules around O_2^-, which dissociates from O_4^-. In the case of $n=8-10$, the gradient for the shift (solid lines in Fig. 8) is much steeper than that of $(O_2)_6^-$ and $(O_2)_7^-$. This efficient evaporation is because in these clusters of a more complete solvent shell, the probability of hard collisions increases between the dissociating O_2^- and the solvent. The efficient energy transfer through these hard collisions rapidly heats up the solvent cage, which in turn makes effective evaporation of solvent molecules.[41] The increase in EBE at a 2–4 ps time delay for $n=8-10$ indicates the onset for recombination. Following the collision with the solvent cage, the O_2^- encounters the other O_2 and reforms O_4^-. The shift toward higher EBE, which approaches the asymptote at 10–20 ps, represents the bond reformation (recombination) and subsequent vibrational relaxation.

The recombination occurs at 2.5 ps for $(O_2)_{10}^-$ and at about 4 ps for $(O_2)_8^-$ and $(O_2)_9^-$. The time constant for effective vibrational relaxation also shows strong size dependence: 12 ps for $(O_2)_8^-$, 4 ps for $(O_2)_9^-$, and 3 ps for $(O_2)_{10}^-$. This is because the larger number of solvent molecules around the reformed O_4^- provides an efficient energy bath with more density of states.[42] The increase in the recombination rate for the larger clusters and the change in vibrational relaxation were observed in other systems.[9,43]

Direct dissociation of O_4^- is primarily responsible for the recombination because the recombination time of $(O_2)_{10}^-$ (2.5 ps) is much shorter than the corresponding τ_2 (8.0 ps). Moreover, the recombination shows a threshold dependence on the cluster size, only observed for the cluster size of $n \geqslant 8$. The time scale for bond breakage is critical for the subsequent recombination and solvent reorganization, as pointed out in the study made in this laboratory on iodine-rare gas clusters.[15–17] A slow dissociation gives solvent molecules enough time to absorb the energy, in this case of dissociating O_2^-, which softens the solvent wall; this soft solvent cage becomes ineffective to force the O_2^- back for recombination.

Johnson and his co-workers[44] recently reported that there exists a bound electronic excited state of O_4^-. However, we suggest that the recombination process, which is reflected as a peak shift in Fig. 8, occurs along the ground potential energy surface for the following reasons; First, the dissociation asymptote of the electronic excited state is about 0.21 eV ($1676\ cm^{-1}$) above that of the repulsive state. Therefore, the nonadiabatic transition from the repulsive state to the electronic excited state near the solvent wall is not likely to occur. Second, the excited state is located a little above the asymptote of the repulsive state. Hence, even though the recombination on the electronic excited state is possible through the curve crossing from the repulsive state following the collision with the solvent wall, the recombination process on this excited state will give rise to a small change in the peak position of the fragment photoelectron spectrum and will not reproduce the behavior in Fig. 8. Finally, vibrational or electronic predissociation, which begins at $\sim 242\ cm^{-1}$ above the band origin of the excited state, will make the recombination on this state much less efficient. If some trajectories of recombination occurs on the excited surface, then internal conversion to the ground state must be ultrafast in order to account for the results.

The striking feature observed in the recombination of O_4^- is that the rate of recombination is significantly slower than those found in other vdW clusters, given the fact that $(O_2)_n^-$, $n \geqslant 7$ has a complete solvent shell; we studied $(O_2)_{13}^-$, and the behavior is still similar to that of $(O_2)_{10}^-$. The prompt recombination was observed in vdW clusters of $I_2(Ar)_n$, $n=8-40$ (660 fs),[16] and the recombination began at 1 ps for $I_2^-(Ar)_{20}$[8,41] and 500 fs for $I_2^-(CO_2)_{16}$,[9] where the first solvent shell is complete. Considering the significant quadrupole moment and the stronger binding energy of O_2, than that of Ar (the binding energy of O_2 in $O_4^- \cdot O_2$ is ~ 0.1 eV, while that of Ar in $I_2^- \cdot Ar$ is 0.052 eV[8]), we can conclude that the solvent wall of O_2 molecules is stiffer and more cohesive than that of Ar. Thus, binding is not the cause of slow recombination.

We suggest that the slow recombination is due to the reorientation process of both O_2^- and O_2 to acquire the proper configuration for O_4^- reformation. Unlike recombination in the case of atoms, the recombination in the case involving two molecules (O_2 and O_2^-) requires a second coordinate, namely the angle (θ) between the two molecules involved. We present a schematic of this dependence in Fig. 12. The nonadiabatic transition between the O_4^- repulsive surface (excited) and bound surface (ground) is θ dependent and hence the transition to the ground state not only depends on the energetics in the asymptote region but also on the relative orientation. The reorientation may occur with a relatively small energy change. However, the friction exerted by ion-induced dipole interaction between O_2^- and the solvent O_2 molecules may slow down the reorientation process.

V. CONCLUSION

In this contribution, we presented studies of the ultrafast dissociation and recombination dynamics of homogeneous O_2^- clusters, from O_6^- to O_{20}^-, using fs, time-resolved photoelectron spectroscopy. Dissociation and recombination of the mass-selected anionic clusters show solvation effects on two different time scales and dissociation pathways—a bifurcation of the wave packet in two channels of direct dissociation and vibrational predissociation. The emergence of bulk properties from clusters was examined and compared with theory—bulk-type behaviors were deduced from the correlation between vertical detachment energy, or adiabatic electron affinity, and the inverse radius of the cluster, $n^{-1/3}$. For the rates we found a dependence on the radius, $n^{1/3}$, and we related such striking behavior to the dynamics of electron recombination in the direct dissociation process. For vibrational dissociation, the solvent evaporation process, the experimental rates show reasonable agreement with the calculated values using a statistical theory. The reformation of the bond in solvent cages becomes evident as the cluster size increases. Our fs time resolution provides the time scale for the recombination and subsequent vibration relaxation, which vary with the cluster size. The measured rates reveal the unique feature in the recombination process between molecules, which is absent in the (atom+atom) bond refor-

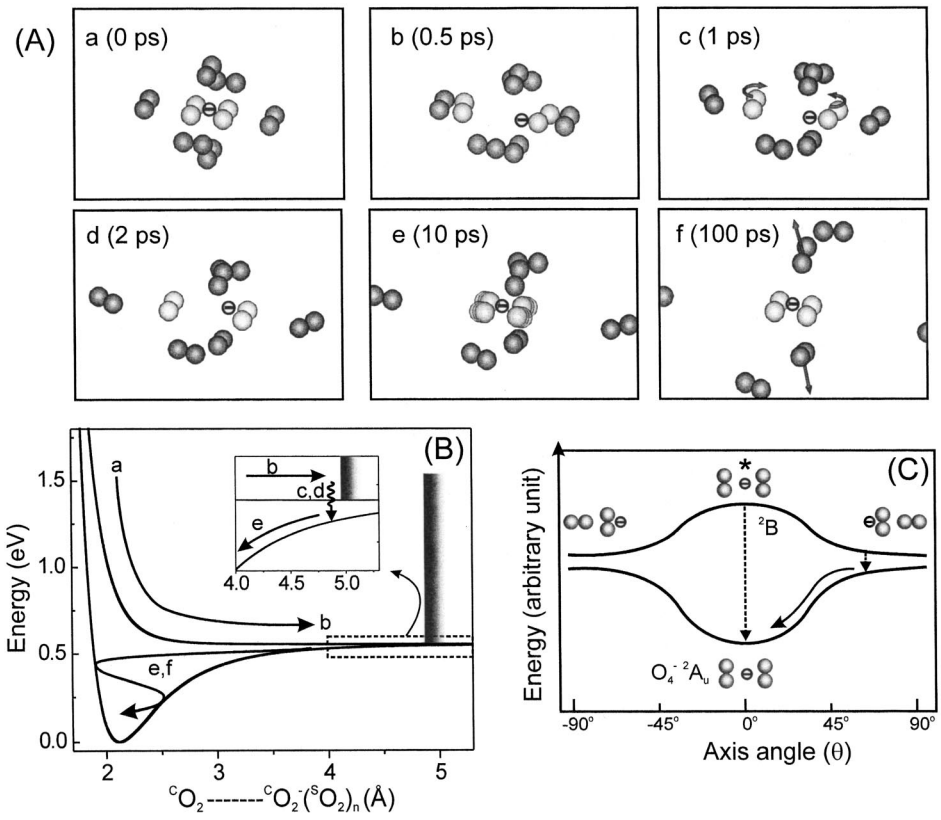

FIG. 12. A schematic representation of the dissociation and recombination dynamics in the O_{20}^- cluster. (a) The representation of snapshots at different times. The corresponding positions of the six frames are indicated on the potential energy surface in (b). The potential energy surface is sketched along the nuclear coordinate of forming O_4^-. The $^{C}O_2$ and $^{S}O_2$ represent the core O_2 and the solvent O_2, respectively. The solvent wall is represented by a shaded bar. (c) A schematic diagram for the energetics of O_2^- and O_2 as a function of the angle between their molecular axes. The intermolecular distance is fixed to where the solvent wall is located. The dotted arrows represent the nonadiabatic transition from the repulsive surface to the ground state (^2A_u) of O_4^-. The solid arrow describes the reorientation process.

mation. The time scale for bond breakage is critical to the rate of bond reformation, and molecular orientations and solvent friction play a significant role, especially at longer times, longer than 1 ps.

ACKNOWLEDGMENTS

This work was supported by the National Science Foundation and the AFOSR. We wish to thank the referee for the thorough reading of the two manuscripts and for helpful comments.

[1] J. Franck and E. Rabinowitsch, Trans. Faraday Soc. **30**, 120 (1934).
[2] C. Lienau and A. H. Zewail, J. Phys. Chem. **100**, 18629 (1996), and references therein.
[3] A. Materny, C. Lienau, and A. H. Zewail, J. Phys. Chem. **100**, 18650 (1996), and see the most recent Ref. 4.
[4] J. Larsen, D. Madsen, J.-A. Poulsen, T. D. Poulsen, S. R. Keiding, and J. Thøgersen, J. Chem. Phys. **116**, 7997 (2002).
[5] M. L. Alexander, N. E. Levinger, M. A. Johnson, D. Ray, and W. C. Lineberger, J. Chem. Phys. **88**, 6200 (1988).
[6] J. M. Papanikolas, J. R. Gord, N. E. Levinger, D. Ray, V. Vorsa, and W. C. Lineberger, J. Phys. Chem. **95**, 8028 (1991).
[7] B. J. Greenblatt, M. T. Zanni, and D. M. Neumark, Science **276**, 1675 (1997).
[8] B. J. Greenblatt, M. T. Zanni, and D. M. Neumark, J. Chem. Phys. **111**, 10566 (1999).
[9] B. J. Greenblatt, M. T. Zanni, and D. M. Neumark, J. Chem. Phys. **112**, 601 (2000).
[10] A. Sanov, T. Sanford, S. Nandi, and W. C. Lineberger, J. Chem. Phys. **111**, 664 (1999).
[11] F. G. Amar and L. Perera, Z. Phys. D: At., Mol. Clusters **20**, 173 (1991).
[12] V. S. Batista and D. F. Coker, J. Chem. Phys. **106**, 7102 (1997).
[13] R. Parson, J. Faeder, and N. Delaney, J. Phys. Chem. **104**, 9653 (2000).
[14] J. Ka and S. Shin, J. Chem. Phys. **109**, 10087 (1998).
[15] Q. Liu, J.-K. Wang, and A. H. Zewail, Nature (London) **364**, 427 (1993).
[16] J.-K. Wang, Q. Liu, and A. H. Zewail, J. Phys. Chem. **99**, 11309 (1995).
[17] Q. Liu, J.-K. Wang, and A. H. Zewail, J. Phys. Chem. **99**, 11321 (1995).
[18] D. H. Paik, N. J. Kim, and A. H. Zewail, J. Chem. Phys. **118**, 6923 (2002).
[19] D. H. Paik, T. M. Bernhardt, N. J. Kim, and A. H. Zewail, J. Chem. Phys. **115**, 612 (2001).
[20] M. J. DeLuca, C.-C. Han, and M. A. Johnson, J. Chem. Phys. **93**, 268 (1990).
[21] R. N. Barnett, U. Landman, C. L. Cleveland, and J. Jortner, Chem. Phys. Lett. **145**, 382 (1988).
[22] M. J. DeLuca, B. Niu, and M. A. Johnson, J. Chem. Phys. **88**, 5857 (1988).
[23] K. Hiraoka, J. Chem. Phys. **89**, 3190 (1988).
[24] The fragments $(O_2)_3^-$ and $(O_2)_4^-$, as well as O_2^- and O_4^-, were observed in the dissociation of parent $(O_2)_{13}^-$.
[25] L. A. Posey and M. A. Johnson, J. Chem. Phys. **88**, 5383 (1988).
[26] K. Ohta and K. Morokuma, J. Phys. Chem. **91**, 401 (1987).
[27] P. Y. Cheng, D. Zhong, and A. H. Zewail, J. Chem. Phys. **105**, 6216 (1996).
[28] S. T. Arnold, J. H. Hendricks, and K. H. Bowen, J. Chem. Phys. **102**, 39 (1995).
[29] J. Jortner, Z. Phys. D: At., Mol. Clusters **24**, 247 (1992).
[30] *CRC Handbook of Chemistry and Physics*, 82nd ed., edited by D. R. Lide (CRC, Boca Raton, FL, 2001), pp. 6–139, 6–152.
[31] C. Wan, T. Fiebig, O. Schiemann, J. K. Barton, and A. H. Zewail, Proc. Natl. Acad. Sci. U.S.A. **97**, 14052 (2000).
[32] A. Ponce, H. B. Gray, and J. R. Winkler, J. Am. Chem. Soc. **122**, 8187 (2000).
[33] N. E. Miller, M. C. Wander, and R. J. Cave, J. Phys. Chem. A **103**, 1084 (1999).
[34] A. García-Vela, P. Villarreal, and G. Delgado-Barrio, J. Chem. Phys. **94**, 7868 (1991).
[35] M. Gutmann, D. M. Willberg, and A. H. Zewail, J. Chem. Phys. **97**, 8048 (1992).
[36] S. Fernandez Alberti, N. Halberstadt, J. A. Beswick, A. Bastida, J. Zúñiga, and A. Requena, J. Chem. Phys. **111**, 239 (1999).
[37] D. M. Willberg, M. Gutmann, J. J. Breen, and A. H. Zewail, J. Chem. Phys. **96**, 198 (1992).
[38] B. Miguel, A. Bastida, J. Zúñiga, A. Requena, and N. Halberstadt, Faraday Discuss. **118**, 257 (2001).

[39] P. J. Robinson and K. A. Holbrook, *Unimolecular Reactions* (Wiley, New York, 1972).
[40] M. J. Frisch, G. W. Trucks, H. B. Schlegel *et al.*, GAUSSIAN 98, Revision A.9, Gaussian, Inc., Pittsburgh, PA, 1998.
[41] J. Faeder and R. Parson, J. Chem. Phys. **108**, 3909 (1998).
[42] The difference in the asymptotes at a 400 ps time delay [1.47 eV for $(O_2)_8^-$, 1.52 eV for $(O_2)_9^-$, and 1.61 eV for $(O_2)_{10}^-$] could be due to the degree of vibrational relaxation in different-sized clusters. However, considering the time constants for vibrational relaxation by solvent O_2 molecules (3–12 ps) and also the number of vibrational modes in O_4^-, an incomplete vibrational relaxation of O_4^- at 400 ps is unlikely. We suggest that the difference is due to the different contribution of the recombined product. It should be noted that the photoelectron spectrum of fragment anions is the sum of a nascent fragment $O_2^-(O_2)_m$ from the dissociation and the $O_4^-(O_2)_k$ from the recombination, each with a different VDE value. The increased production of recombined $O_4^-(O_2)_k$ in larger clusters makes the asymptote value shifts toward higher EBE.
[43] V. Vorsa, S. Nandi, P. J. Campagnola, M. Larsson, and W. C. Lineberger, J. Chem. Phys. **106**, 1402 (1997).
[44] J. A. Kelley, W. H. Robertson, and M. A. Johnson, Chem. Phys. Lett. **362**, 255 (2002).